(Cd,Zn,Mg)Te-based microcavity on MgTe sacrificial buffer: Growth, lift-off, and transmission studies of polaritons

B. Seredyński,[1,*] M. Król,[1] P. Starzyk,[1] R. Mirek,[1] M. Ściesiek,[1] K. Sobczak,[2] J. Borysiuk,[1] D. Stephan,[1] J.-G. Rousset,[1] J. Szczytko,[1] B. Piętka,[1] and W. Pacuski[1]

[1]*Institute of Experimental Physics, Faculty of Physics, University of Warsaw, ul. Pasteura 5, 02-093 Warsaw Poland*

[2]*Biological and Chemical Research Centre, Faculty of Chemistry, University of Warsaw, ul. Żwirki i Wigury 101, 02-089 Warsaw, Poland*

(Received 10 November 2017; published 26 April 2018)

Opaque substrates precluded, so far, transmission studies of II-VI semiconductor microcavities. This work presents the design and molecular beam epitaxy growth of semimagnetic (Cd,Zn,Mn)Te quantum wells embedded into a (Cd,Zn,Mg)Te-based microcavity, which can be easily separated from the GaAs substrate. Our lift-off process relies on the use of a MgTe sacrificial layer which stratifies in contact with water. This allowed us to achieve a II-VI microcavity prepared for transmission measurements. We evidence the strong light-matter coupling regime using photoluminescence, reflectivity, and transmission measurements at the same spot on the sample. By comparing a series of reflectance spectra before and after lift-off, we prove that the microcavity quality remains high. Thanks to Mn content in quantum wells we show the giant Zeeman splitting of semimagnetic exciton-polaritons in our transmitting structure.

DOI: 10.1103/PhysRevMaterials.2.043406

I. INTRODUCTION

Cavity exciton-polaritons [1] are quasiparticles exhibiting fascinating phenomena such as Bose-Einstein condensation [2,3] and superfluidity [4]. Recently, there is a growing interest in the magnetooptical properties of cavity exciton-polaritons and their condensates [5–9], e.g., magnetic field tuning of spin levels paves the way to investigate polariton bistability [10] and spin multistability [11]. In this context, II-VI based microcavities are of particular interest since they allow to combine the magnetooptical properties of excitons in diluted magnetic semiconductors with cavity polaritons [12–18] giving rise to semimagnetic cavity polaritons [19–23]. In such a system, the enhanced magnetooptical properties of polaritons are inherited from their excitonic part and result in an angle-dependent giant Zeeman splitting [21] and a decrease of the polariton lasing threshold in a magnetic field [22]. In order to investigate the properties of a semimagnetic polariton superfluid in a magnetic field, a sample allowing for transmission measurements is the most beneficial [4]. Although the transparent substrates are commercially available, they are not produced in sufficient sizes and the growth of the desire structure is challenging [24–26]. Another approach consists of growing a sacrificial layer between the microcavity structure and the GaAs substrate, which is removed in a postgrowth process. This method has proved to be efficient in the case of chemical resistant structures [27–34]. Here, we present a lift-off method developed for potentially unstable and hygroscopic magnesium compounds. Our method results in the production of a microcavity containing three semimagnetic (Cd,Zn,Mn)Te quantum wells (QW) enabling transmission measurements. Our optical investigation shows that after the lift-off process the microcavity properties are not undermined and the strong coupling regime is still present. Our magnetooptical measurements reveal the giant Zeeman effect of the semimagnetic cavity polaritons. Our results are an important milestone towards the investigation of the magnetooptical properties of semimagnetic polariton superfluids.

II. TECHNOLOGY

A. Molecular beam epitaxy growth

Using molecular beam epitaxy on a 3" (100)-oriented GaAs:Si substrate, we have grown a 1-μm-thick CdTe buffer and a 1-μm hygroscopic MgTe layer. Typically, Mg-based II-VI compounds crystallize in the rock salt or wurtzite structure [35], but the metastable zinc-blende structure can be obtained by growing epitaxially the Mg-based compound on a (100)-oriented zinc-blende substrate [36–38]. In our case, MgTe inherits its zinc-blende structure from the CdTe buffer. The reduced lattice mismatch of MgTe-CdTe compared to MgTe-GaAs ensures good growth conditions for MgTe. As shown in Fig. 1, the microcavity itself consists of (Cd,Zn,Mg)Te layers with various Mg concentration and is lattice matched to MgTe, assuring the refractive index contrast in the distributed Bragg reflector (DBR) layers and keeping the lattice constant unchanged [20,39–41]. Both DBRs, bottom and top, consist of 22 pairs made of $Cd_{0.61}Zn_{0.06}Mg_{0.33}Te$ for low refractive index layers and $Cd_{0.84}Zn_{0.08}Mg_{0.08}Te$ for high refractive index layers. The determination of the Mg concentration in DBRs is based on both the absorption edge energy of the presented system and the analysis of the refractive index described in detail in Sec. III. The $Cd_{0.84}Zn_{0.08}Mg_{0.08}Te$ cavity has a λ_0/n optical thickness with $\lambda_0 = 760$ nm, corresponding to the cavity resonance at the center of the DBRs stopband and near the QWs emission. Three $Cd_{0.91}Zn_{0.088}Mn_{0.002}Te$ quantum wells are placed at the antinode of the electric field standing

*Bartlomiej.Seredynski@fuw.edu.pl

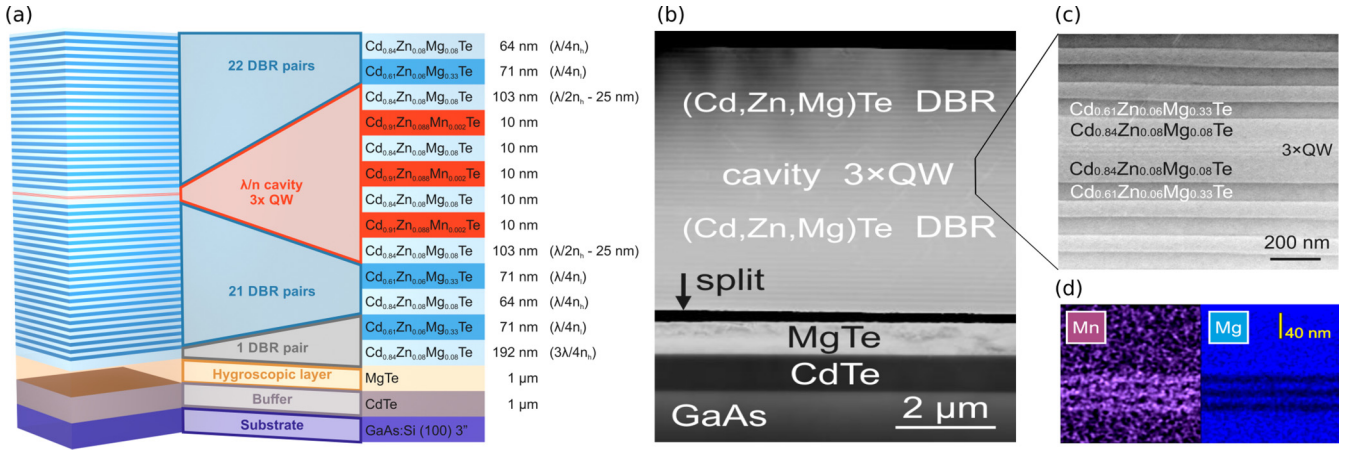

FIG. 1. (a) Sample structure with the nominal layers thickness. (b) Scanning transmission electron microscope (STEM) image of the sample schematically presented in (a). (c) Close-up of the cavity region with the (Cd,Zn,Mn)Te QWs. (d) Presence of Mn in QWs and Mg in barriers revealed by energy x-ray spectroscopy in STEM configuration.

wave in the center of the cavity in order to maximize the coupling between QW excitons and cavity photons. The Zn content is estimated based on the QWs emission energy [42] and the Mn content is estimated from the giant Zeeman effect according to Ref. [43]. The presence of Zn in DBRs and QWs reduces strain and the presence of Mn^{2+} ions in the QWs enhances the magnetooptical properties of the polaritons through the s, p-d exchange interaction.

During the growth process, the sample is not rotated, which results in a wedgelike shape for the cavity and DBRs. This allows different light wavelengths to be confined in the cavity at different positions in the sample. As a result, we are able to tune our structure through a wide range of cavity mode wavelengths around the photon-exciton resonance.

B. Lift-off process

In order to isolate the microcavity structure from the GaAs substrate and CdTe buffer, the epitaxial face of the sample is glued to a quartz plate with a neoprene glue and immersed in deionized water at room temperature. During this rinsing step, schematically presented in Fig. 2, MgTe in the thick sacrificial layer reacts with water, dissociating in $Mg(OH)_2$ and H_2Te, which results in a stratification of the MgTe sacrificial layer and consequently disjoints the substrate from the microcavity structure glued on the quartz plate. After immersion, the sample is dried in nitrogen flow to avoid further sample degradation, and a small effort is needed to mechanically separate the

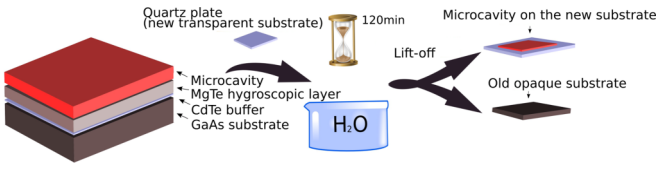

FIG. 2. Sketch of the lift-off procedure. The microcavity structure is grown on a hygroscopic MgTe buffer and its epitaxial face is glued to a quartz plate. After 2-hour rinsing in deionized water, it is dried with pressurized nitrogen and mechanically removed from the opaque GaAs substrate.

microcavity on the quartz plate from the substrate. Various immersion times have been tested from 15 minutes to 24 hours. We find that for our structure formed on 1-μm-thick MgTe the optimal immersion time is about 2 hours, which allows to obtain a lifted-off structure with the best homogeneity. As can be seen in Fig. 3(a) after our lift-off process, we obtain homogeneous flakes with a characteristic area of more than 2 mm^2, which is enough for both preliminary studies and potential devices. Shorter times do not allow for lift-off after drying and longer times affect the microcavity structure as revealed by optical microscopy characterization shown in Fig. 3(b). It is worth noticing that the hygroscopic layer is ten times thicker compared to our previous work performed on exfoliated QDs [34]. In the latter work, the sample was immersed for 24 hours and then we could proceed with the exfoliation-like lift-off of the QDs. In the present work, the microcavity structure presents a risk of degradation during immersing in water due to the presence of magnesium compounds in each of its layers and therefore the immersion time had to be reduced. We observe, indeed, that increasing the immersion time makes the lift-off easier, however, the microcavity molders at the same time.

III. OPTICAL SPECTROSCOPY

A. Room-temperature transmission and reflectivity

Optical transmission investigations were performed after lift-off of the microcavity from the substrate and the buffer. In Fig. 4, we compare the transmittance and the reflectance spectra, both measured at room temperature. The high reflectance spectral range between 1.38 and 1.48 eV called stopband corresponds to a transmittance minimum. The cavity mode is visible at center of the stop-band as a minimum (maximum) of the signal in the reflectivity (transmission) spectra. Side oscillations result from interference in the multiple layers of the DBRs. The experimental data are fitted using the transfer matrix formalism [44,45] (red solid lines in Fig. 4). In our model, the refractive index values of the (Cd,Zn,Mg)Te layers are approximated by literature data of (Cd,Mg)Te layers given in Ref. [46]. The Mg content in the low energy gap (high refractive index) $Cd_{0.84}Zn_{0.08}Mg_{0.08}Te$ was evaluated basing

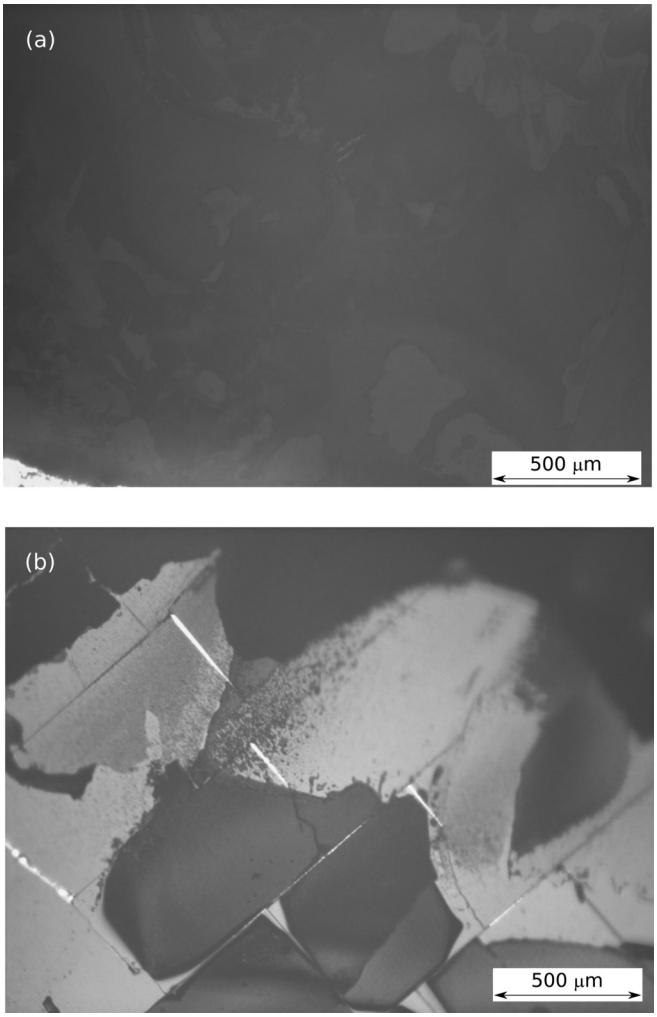

FIG. 3. Sample surface characterization by optical microscope in transmission mode. (a) Best surface homogeneity is achieved after a 2-hour immersion time—continuous area of more than 2 mm^2 can be seen; edge of the sample at the bottom left corner of the image. (b) Too long immersion time (24-hours) results in holes torn out within the sample.

on the energy gap determined from Fig. 4(b) ($E_{g(\mathrm{low})} = 1.7$ eV), taking into account an energy gap increase of about 18.5 meV for each percent of Mg [37], and an energy gap increase related to Zn content, as determined from observation of (Cd,Zn)Te QWs. On this basis, the Mg content in the high energy gap (low refractive index) $Cd_{0.61}Zn_{0.06}Mg_{0.33}Te$ layer is used as a fitting parameter adjusting the stop-band width, which is governed by the refractive index step in the DBR layers.

B. Low-temperature reflectivity: Strong coupling

In order to study the exciton-photon coupling in our microcavity structure, we performed reflectance measurements at helium temperatures ($T = 7$ K). The experiment was set on the same cleaved part of the sample before and after the lift-off process. Taking advantage of the wedgelike shape of the layers resulting from the growth process, we have collected a series of reflectance spectra for various cavity mode energies,

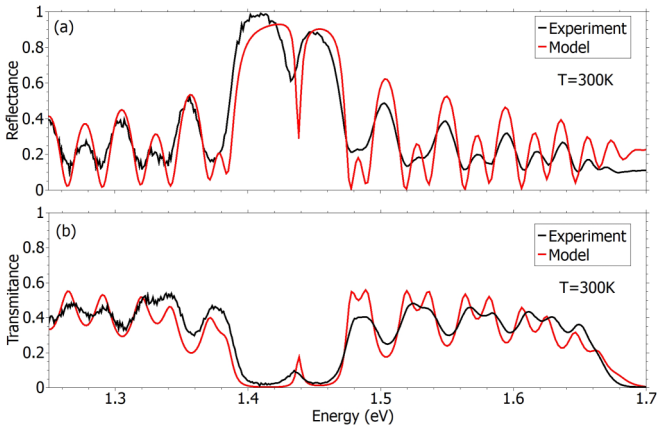

FIG. 4. Reflectance (a) and transmittance (b) spectra measured at room temperature. A stopband is observed between 1.38 and 1.48 eV. The cavity mode is at 1.43 eV. Side oscillations result from interference in the multiple layers of the DBRs. Red solid lines represent the fit using the transfer matrix method taking into account the refractive index dispersion.

i.e., exciton-photon detuning values. As can be seen in Fig. 5 when probing various places at the sample surface along the thickness gradient, the whole spectra (stop-band, cavity mode, and side-band oscillations) drifts in energy from higher to

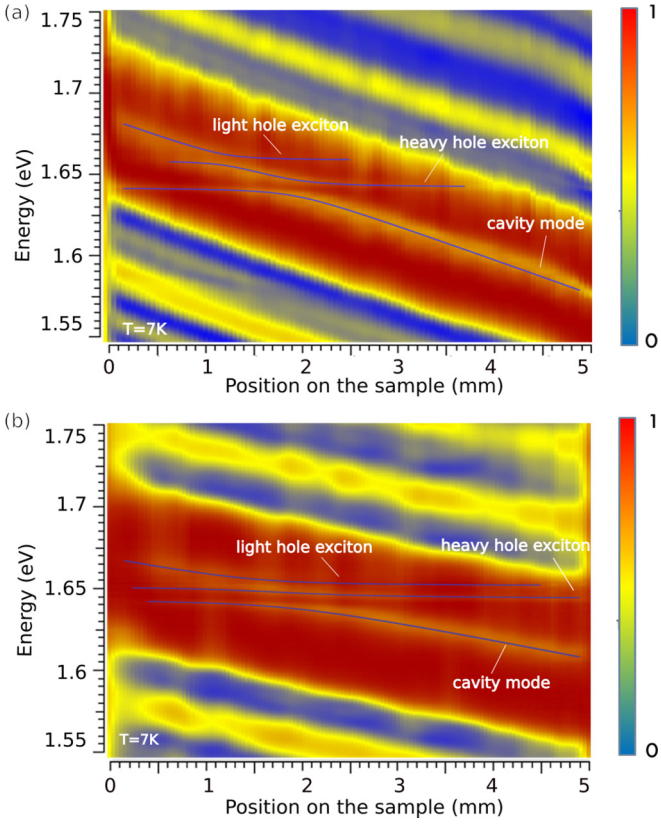

FIG. 5. Reflectivity maps before (a) and after (b) lift-off measured at 7 K reveal the strong exciton-photon coupling, thus the formation of exciton-polaritons. Solid lines represent model based on exciton-photon interaction Hamiltonian (1).

lower values compared to the both heavy and light hole QW excitons. When the energy of the cavity mode is close to the QW excitons, around 1.65 eV, we observe clear anticrossing behavior, which is a signature of the strong exciton-photon coupling and the formation of exciton-polaritons. Comparing the reflectance maps before and after the lift-off process [Figs. 5(a) and 5(b), respectively], it is clear that the strong coupling regime is still present after lift-off, which proves that the lift-off process does not significantly alter the microcavity structure despite the relatively high Mg concentration in the DBR layers. We attribute the little difference in dependence of the stop-band energy on the position to the fact that we probe a slightly different position on the sample before and after lift-off. Solid blue lines in Fig. 5 represent the solution of the time independent Schrödinger equation for the interaction Hamiltonian between both heavy- and light-hole excitons and photons:

$$H = \begin{bmatrix} E_{ph} & \omega_{hh}/2 & \omega_{lh}/2 \\ \omega_{hh}/2 & E_{hh} & 0 \\ \omega_{lh}/2 & 0 & E_{lh} \end{bmatrix}, \quad (1)$$

where E_{ph} is the confined photon energy which is being changed during scan, E_{hh} and E_{lh} are the energies of heavy-hole and light-hole excitons, respectively, ω_{hh} and ω_{lh} are the coupling energies of heavy-hole and light-hole excitons, respectively, with a photon. We do not observe a significant effect of the lift-off procedure on the parameters E_{hh}, ω_{hh}, and ω_{lh}. Those fitting parameter values are $E_{hh} = 1643.0$ meV, $\omega_{hh} = 10.6$ meV, $\omega_{lh} = 7.4$ meV and $E_{hh} = 1643.8$ meV, $\omega_{hh} = 10.3$ meV, $\omega_{lh} = 8.5$ meV for before and after lift-off, respectively. We, however, notice that some of the system parameters have changed after the lift-off process, e.g., the light-hole exciton energy decreased from 1660.4 to 1652.2 meV. Since the light-hole exciton energy is particularly sensitive to strain, we conclude that the strain of the sample induced by cooling process on GaAs and glass substrate is different. Also the full width at half maximum (FWHM) of the cavity mode decreases from 5.97 to 5.32 meV, which can be interpreted as an increase of cavity quality factor due to suppression of the absorption after removing the absorbing CdTe buffer and GaAs substrate and improvement of the reflectance on the air/semiconductor interface comparing to the (Cd,Zn,Mg)Te/MgTe interface.

C. Polariton dispersion

To observe the polariton dispersion in our lifted-off structure, we performed measurements resolved by the angle of emission. For that purpose, we collected the signal from the sample in a far-field configuration (k-space imaging) at helium temperatures ($T = 7$ K). We investigated two positions at the sample surface corresponding to two different values of the exciton-photon detuning. Results of k-space measurements of back illuminated photoluminescence presented in Figs. 6(a) and 6(d) reveal various behaviors of polaritons in the presented system. For a slightly negative detuning $\delta = -3.6$ meV [Fig. 6(a)], we observe that polariton recombination occurs mainly at the bottom of the lower polariton dispersion curve, for a more negative detuning $\delta = -15.3$ meV [Fig. 6(d)], the polariton recombination occurs mainly at the so-called

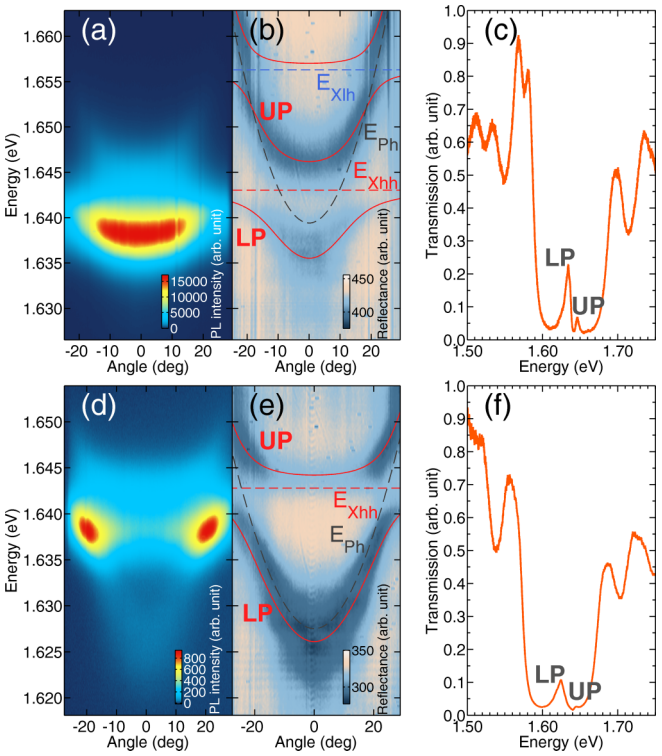

FIG. 6. Low-temperature angle-resolved back excited photoluminescence [(a) and (d)], angle-resolved reflectance [(b) and (e)], and real-space transmittance at normal incidence [(c) and (f) [for two different detuning values $\delta = -3.6$ meV [(a)–(c)] and $\delta = -15.3$ meV [(d)–(f)].

bottleneck of the lower polariton. Despite the relatively strong signal observed for negative detuning, polariton condensation was not observed due to a heat dissipation in our sample with only three 10-nm-thick QWs. This is in agreement with the fact that for samples we have grown without a MgTe buffer, the lowest number of QWs required for condensation was 4 (20-nm QWs) [20,22]. The values of exciton-photon detuning are determined thanks to the lower and upper polariton dispersion curves measured using angle-resolved reflectance [Figs. 6(b) and 6(e)] and fitted using Hamiltonian (1) including the angular dependence of the cavity photon energy. Transmittance spectra at normal angle ($k = 0$), presented in Figs. 6(c) and 6(f) also allow to identify the lower and upper polariton resonances.

D. Giant Zeeman effect for polaritons

Figure 7(a) shows photoluminescence spectra measured in magnetic field up to 5 T, in Faraday configuration, in two circular polarizations, at low temperature ($T = 7$ K). Two polariton peaks corresponding to lower and upper polaritons can be resolved. Their position as a function of magnetic field is plotted in Fig. 7(b). We observe significant splitting of both polariton states, as expected for semimagnetic polaritons [21]. Since the total (uncoupled) exciton wave function is distributed over the polaritons, the sum of the lower and upper polariton splitting gives the Zeeman splitting of the uncoupled exciton [47], which allows to evaluate [43] the Mn content in the QWs to $x = 0.2\%$. Worth noticing is the fact that typically

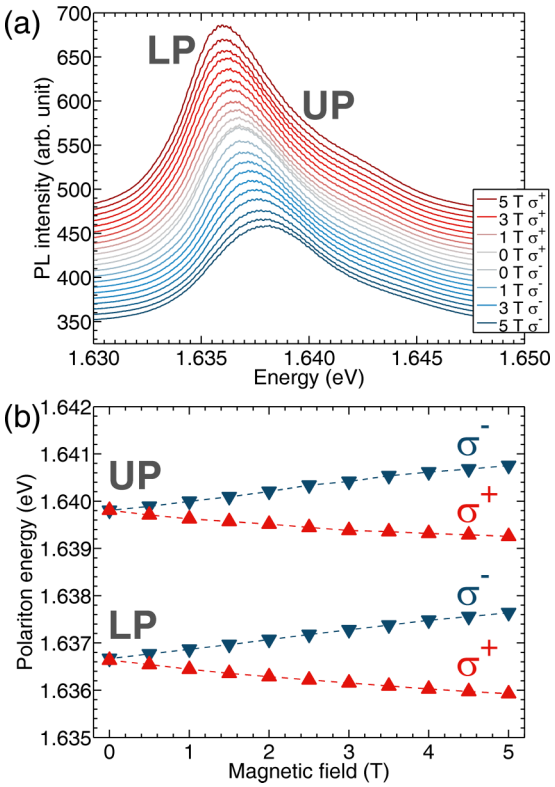

FIG. 7. Magnetophotoluminescence at normal incidence performed at $T = 7$ K reveals a giant Zeeman effect of polaritons proving the presence of Mn^{2+} ions in the microcavity. (a) Photoluminescence spectra measured in Faraday configuration, in two circular polarizations. Magnetic field step size is 0.5 T. (b) Energy position of the lower and upper polaritons as a function of magnetic field. The sum of the energy splitting for the lower and upper polaritons gives information on the Mn^{2+} ions content in the sample.

several tens of μeV splitting in several teslas is observed, while in our sample this value is about 2 meV at 5 T.

IV. CONCLUSIONS

In this work, we have presented a lift-off method, which allowed to obtain a microcavity designed for transmission investigation of semimagnetic cavity polaritons. The lift-off process relies on a MgTe sacrificial layer that dissociates in water. The immersion time of the sample in water is a crucial parameter and we show that for a 1-μm-thick sacrificial MgTe layer an optimal 2 hour immersion time allows to easily separate the microcavity from the GaAs substrate and does not undermine the cavity optical parameters neither the exciton-photon strong coupling. Low-temperature transmission measurements and angle-resolved reflectance and back illuminated photoluminescence evidence the polaritons dispersion. Our magnetooptical investigation shows the giant Zeeman splitting of semimagnetic cavity polaritons. These results are an important milestone toward the study of magnetooptical properties of superfluid cavity polaritons for which transmitting samples are needed.

ACKNOWLEDGMENTS

The authors acknowledge Michał Nawrocki and Piotr Kossacki for helpful discussions. This work was supported by the Polish National Science Centre under decisions DEC-2015/18/E/ST3/00559, 2015/18/E/ST3/00558, and DEC-2014/13/N/ST3/03763. This study was carried out with the use of CePT, CeZaMat, NLTK, and CNBCH infrastructures financed by the European Union - the European Regional Development Fund.

[1] C. Weisbuch, M. Nishioka, A. Ishikawa, and Y. Arakawa, Observation of the Coupled Exciton-Photon Mode Splitting in a Semiconductor Quantum Microcavity, Phys. Rev. Lett. **69**, 3314 (1992).

[2] H. Deng, G. Weihs, C. Santori, J. Bloch, and Y. Yamamoto, Condensation of semiconductor microcavity exciton polaritons, Science **298**, 199 (2002).

[3] J. Kasprzak, M. Richard, S. Kundermann, A. Baas, P. Jeambrun, J. M. J. Keeling, F. M. Marchetti, M. H. Szymańska, R. André, J. L. Staehli, V. Savona, P. B. Littlewood, B. Deveaud, and Le Si Dang, Bose-Einstein condensation of exciton polaritons, Nature (London) **443**, 409 (2006).

[4] A. Amo, J. Lefrère, S. Pigeon, C. Adrados, C. Ciuti, I. Carusotto, R. Houdré, E. Giacobino, and A. Bramati, Superfluidity of polaritons in semiconductor microcavities, Nat. Phys. **5**, 805 (2009).

[5] Y. G. Rubo, A. Kavokin, and I. Shelykh, Suppression of superfluidity of exciton-polaritons by magnetic field, Phys. Lett. A **358**, 227 (2006).

[6] J. Fischer, S. Brodbeck, A. V. Chernenko, I. Lederer, A. Rahimi-Iman, M. Amthor, V. D. Kulakovskii, L. Worschech, M. Kamp, M. Durnev, C. Schneider, A. V. Kavokin, and S. Höfling, Anomalies of a Nonequilibrium Spinor Polariton Condensate in a Magnetic Field, Phys. Rev. Lett. **112**, 093902 (2014).

[7] B. Piętka, D. Zygmunt, M. Król, M. R. Molas, A. A. L. Nicolet, F. Morier-Genoud, J. Szczytko, J. Łusakowski, P. Zięba, I. Tralle, P. Stępnicki, M. Matuszewski, M. Potemski, and B. Deveaud, Magnetic field tuning of exciton-polaritons in a semiconductor microcavity, Phys. Rev. B **91**, 075309 (2015).

[8] V. P. Kochereshko, D. V. Avdoshina, P. Savvidis, S. I. Tsintzos, Z. Hatzopoulos, A. V. Kavokin, L. Besombes, and H. Mariette, On the condensation of exciton polaritons in microcavities induced by a magnetic field, Semiconductors **50**, 1506 (2016).

[9] B. Piętka, M. R. Molas, N. Bobrovska, M. Król, R. Mirek, K. Lekenta, P. Stępnicki, F. Morier-Genoud, J. Szczytko, B. Deveaud, M. Matuszewski, and M. Potemski, 2*s* exciton-polariton revealed in an external magnetic field, Phys. Rev. B **96**, 081402 (2017).

[10] A. Baas, J. Ph. Karr, H. Eleuch, and E. Giacobino, Optical bistability in semiconductor microcavities, Phys. Rev. A **69**, 023809 (2004).

[11] S. S. Gavrilov, A. V. Sekretenko, N. A. Gippius, C. Schneider, S. Höfling, M. Kamp, A. Forchel, and V. D. Kulakovskii, Spin multistability of cavity polaritons in a magnetic field, Phys. Rev. B **87**, 201303 (2013).

[12] H. Ulmer-Tuffigo, F. Kany, G. Feuillet, R. Langer, J. Bleuse, and J. Pautrat, Magnetic tuning of resonance in semimagnetic semiconductor microcavities, J. Cryst. Growth **159**, 605 (1996).

[13] J. Sadowski, H. Mariette, A. Wasiela, R. André, Y. Merle d'Aubigné, and T. Dietl, Magnetic tuning in excitonic Bragg structures of (Cd,Mn)Te/(Cd,Zn,Mg)Te, Phys. Rev. B **56**, R1664 (1997).

[14] M. Haddad, R. André, R. Frey, and C. Flytzanis, Enhanced Faraday rotation in an asymmetric semiconductor microcavity, Solid State Commun. **111**, 61 (1999).

[15] D. P. Cubian, M. Haddad, R. André, R. Frey, G. Roosen, J. L. A. Diego, and C. Flytzanis, Photoinduced magneto-optic Kerr effects in asymmetric semiconductor microcavities, Phys. Rev. B **67**, 045308 (2003).

[16] A. Brunetti, M. Vladimirova, D. Scalbert, and R. André, Spin quantum beats in CdMnTe microcavity, Phys. Status Solidi C **2**, 3876 (2005).

[17] M. Koba and J. Suffczyński, Magneto-optical effects enhancement in DMS layers utilizing 1-D photonic crystal, J. Electromagnet. Wave **27**, 700 (2013).

[18] M. Koba and J. Suffczyński, Angle dependence of photonic enhancement of magneto-optical Kerr effect in DMS layers, Europhys. Lett. **108**, 27004 (2014).

[19] A. Brunetti, M. Vladimirova, D. Scalbert, R. André, D. Solnyshkov, G. Malpuech, I. A. Shelykh, and A. V. Kavokin, Coherent spin dynamics of exciton-polaritons in diluted magnetic microcavities, Phys. Rev. B **73**, 205337 (2006).

[20] J.-G. Rousset, B. Piętka, M. Król, R. Mirek, K. Lekenta, J. Szczytko, J. Borysiuk, J. Suffczyński, T. Kazimierczuk, M. Goryca, T. Smoleński, P. Kossacki, M. Nawrocki, and W. Pacuski, Strong coupling and polariton lasing in Te based microcavities embedding (Cd,Zn)Te quantum wells, Appl. Phys. Lett. **107**, 201109 (2015).

[21] R. Mirek, M. Król, K. Lekenta, J.-G. Rousset, M. Nawrocki, M. Kulczykowski, M. Matuszewski, J. Szczytko, W. Pacuski, and B. Piętka, Angular dependence of giant Zeeman effect for semimagnetic cavity polaritons, Phys. Rev. B **95**, 085429 (2017).

[22] J.-G. Rousset, B. Piętka, M. Król, R. Mirek, K. Lekenta, J. Szczytko, W. Pacuski, and M. Nawrocki, Magnetic field effect on the lasing threshold of a semimagnetic polariton condensate, Phys. Rev. B **96**, 125403 (2017).

[23] P. Miętki and M. Matuszewski, Magnetic polarons in a nonequilibrium polariton condensate, Phys. Rev. B **96**, 115310 (2017).

[24] Y. Wu, L. Zhang, G. Xie, J. Ni, and Y. Chen, Structural and electrical properties of (110) ZnO epitaxial thin films on (001) $SrTiO_3$ substrates, Solid State Commun. **148**, 247 (2008).

[25] C. Jia, Y. Chen, X. Liu, S. Yang, W. Zhang, and Z. Wang, Control of epitaxial relationships of ZnO/$SrTiO_3$ heterointerfaces by etching the substrate surface, Nanoscale Res. Lett. **8**, 23 (2013).

[26] M. Karger and M. Schilling, Epitaxial properties of Al-doped ZnO thin films grown by pulsed laser deposition on $SrTiO_3$ (001), Phys. Rev. B **71**, 075304 (2005).

[27] M. Konagai, M. Sugimoto, and K. Takahashi, High efficiency GaAs thin film solar cells by peeled film technology, J. Cryst. Growth **45**, 277 (1978).

[28] A. Balocchi, A. Curran, T. C. M. Graham, C. Bradford, K. A. Prior, and R. J. Warburton, Epitaxial liftoff of ZnSe-based heterostructures using a II-VI release layer, Appl. Phys. Lett. **86**, 011915 (2005).

[29] C. Bradford, A. Currran, A. Balocchi, B. Cavenett, K. Prior, and R. Warburton, Epitaxial lift-off of MBE grown II-VI heterostructures using a novel MgS release layer, J. Cryst. Growth **278**, 325 (2005).

[30] A. Curran, J. K. Morrod, K. A. Prior, A. K. Kar, and R. J. Warburton, Exciton-photon coupling in a ZnSe-based microcavity fabricated using epitaxial liftoff, Semicond. Sci. Technol. **22**, 1189 (2007).

[31] F. Sotier, T. Thomay, T. Hanke, J. Korger, S. Mahapatra, A. Frey, K. Brunner, R. Bratschitsch, and A. Leitenstorfer, Femtosecond few-fermion dynamics and deterministic single-photon gain in a quantum dot, Nat. Phys. **5**, 352 (2009).

[32] C.-W. Cheng, K.-T. Shiu, N. Li, S.-J. Han, L. Shi, and D. K. Sadana, Epitaxial lift-off process for gallium arsenide substrate reuse and flexible electronics, Nat. Commun. **4**, 1577 (2013).

[33] S. Bieker, P. R. Hartmann, T. Kießling, M. Rüth, C. Schumacher, C. Gould, W. Ossau, and L. W. Molenkamp, Removal of GaAs growth substrates from II-VI semiconductor heterostructures, Semicond. Sci. Technol. **29**, 045016 (2014).

[34] B. Seredyński, P. Starzyk, and W. Pacuski, Exfoliation of epilayers with quantum dots, Materials Today: Proceedings **4**, 7053 (2017).

[35] O. Madelung, *II-VI Compounds*, Semiconductors: Data Handbook (Springer, Berlin, Heidelberg, 2004), pp. 173–244.

[36] A. Waag, H. Heinke, S. Scholl, C. Becker, and G. Landwehr, Growth of MgTe and $Cd_{1-x}Mg_xTe$ thin films by molecular beam epitaxy, J. Cryst. Growth **131**, 607 (1993).

[37] J. M. Hartmann, J. Cibert, F. Kany, H. Mariette, M. Charleux, P. Alleysson, R. Langer, and G. Feuillet, CdTe/MgTe heterostructures: Growth by atomic layer epitaxy and determination of MgTe parameters, J. Appl. Phys. **80**, 6257 (1996).

[38] E. Dynowska, E. Janik, J. Bąęk-Misiuk, J. Domagała, T. Wojtowicz, and J. Kossut, Direct measurement of the lattice parameter of thick stable zinc-blende MgTe layer, J. Alloys Comp. **286**, 276 (1999).

[39] J.-G. Rousset, J. Kobak, T. Slupinski, T. Jakubczyk, P. Stawicki, E. Janik, M. Tokarczyk, G. Kowalski, M. Nawrocki, and W. Pacuski, MBE growth and characterization of a II-VI distributed Bragg reflector and microcavity lattice-matched to MgTe, J. Cryst. Growth **378**, 266 (2013).

[40] J.-G. Rousset, J. Kobak, E. Janik, T. Jakubczyk, R. Rudniewski, P. Piotrowski, M. Ściesiek, J. Borysiuk, T. Slupinski, A. Golnik, P. Kossacki, M. Nawrocki, and W. Pacuski, MBE grown microcavities based on selenium and tellurium compounds, J. Cryst. Growth **401**, 499 (2014).

[41] W. Pacuski, J.-G. Rousset, V. Delmonte, T. Jakubczyk, K. Sobczak, J. Borysiuk, K. Sawicki, E. Janik, and J. Kasprzak, Antireflective photonic structure for coherent nonlinear spectroscopy of single magnetic quantum dots, Cryst. Growth Des. **17**, 2987 (2017).

[42] O. Zelaya-Angel, J. G. Mendoza-Alvarez, M. Becerril, H. Navarro-Contreras, and L. L. Tirado-Mejia, On the bowing parameter in $Cd_{1-x}Zn_xTe$, J. Appl. Phys. **95**, 6284 (2004).

[43] J. A. Gaj, W. Grieshaber, C. Bodin-Deshayes, J. Cibert, G. Feuillet, Y. Merle d'Aubigné, and A. Wasiela, Magneto-optical study of interface mixing in the CdTe-(Cd,Mn)Te system, Phys. Rev. B **50**, 5512 (1994).

[44] P. Yeh, *Optical Waves in Layered Media* (Wiley, New York, 1988).

[45] C. B. Fu, C.-S. Yang, M. C. Kuo, Y. J. Lai, J. Lee J. L. Shen, W. Chou, and S. Jeng, High reflectance ZnTe/ZnSe distributed Bragg reflector at 570 nm, Chin. J. Phys. **41**, 535 (2003).

[46] R. André and Le Si Dang, Low-temperature refractive indices of $Cd_{1-x}Mn_xTe$ and $Cd_{1-y}Mg_yTe$, J. Appl. Phys. **82**, 5086 (1997).

[47] J.-G. Rousset, Microcavities based on selenium and tellurium compounds: Technology, magneto-optical properties and lasing, Ph.D. thesis, Faculty of Physics, University of Warsaw, 2017.